Restoring dispersion cancellation for entangled photons produced by ultrashort pulses

Reinhard Erdmann*
Air Force Research Laboratory, SNDP, Rome, New York 13441

David Branning†
NIST, 100 Bureau Drive, Stop 8441, Gaithersburg, Maryland 20899-8441

Warren Grice*
Department of Physics, Southern Illinois University, Edwardsville, Illinois 62026

I. A. Walmsley
The Institute of Optics, University of Rochester, Rochester, New York 14627

(Received 10 December 1999; revised manuscript received 4 May 2000; published 19 October 2000)

It is a well-known and remarkable fact that in certain coincidence photon-counting experiments with cw-pumped parametric down-converters, the effects of group-velocity dispersion arising from media interposed between source and detectors are completely canceled, even if the media physically affect only one of the photons of the pair. Recently Perina *et al.* [Phys. Rev. A **59**, 2359 (1999)] showed that this phenomenon does not occur when certain classical timing information is available about the arrival of individual photons at the detectors, as is the case when the photon pairs are produced via spontaneous parametric down-conversion using an ultrashort pump pulse. In this paper we show that the nonlocal cancellation of dispersion for such a source of entangled photons can be restored in principle by proper engineering of the source properties. In particular, we describe techniques for recovering interference in coincidence-counting experiments by suppressing distinguishing information without the post selection of photons. Moreover, a precise classical timing signal coincident with the photon pair is still available.

PACS number(s): 42.50.Dv, 42.65.Ky

I. INTRODUCTION

Dispersion plays an important role in the propagation of short classical optical pulses and of quantum wave packets. In particular, transform-limited classical pulses as well as single-photon wave packets experience temporal broadening upon propagating through a dispersive medium. In classical applications such as communication over optical fibers this pulse broadening ultimately limits the data transfer rates, unless appropriate compensation methods are implemented [1]. In the case of quantum communications over fibers [2], the data rates are sufficiently low that such considerations are not necessary. Nonetheless, the presence of dispersive systems in the path between source and detector can compromise certain important quantum phenomena that are central to some of the communications protocols, such as teleportation and dense coding, which rely on entangled photon multiplets.

For example, Bell-state measurement is the key to the entanglement swapping [3] that lies at the heart of teleportation. The method proposed for this measurement by Braunstein and Mann [4] makes use of a Hong-Ou-Mandel (HOM) interferometer [5]. In the HOM interferometer, the paths of two photons are overlapped at a beam splitter and the resulting coincidence counts are monitored. Destructive interference of the two-photon amplitudes produces a ''dip'' in the coincidence counts as the relative path delay between the two photons is varied. According to the Braunstein-Mann protocol, the detection of a coincidence in the center of this ''dip'' allows one to infer that the joint polarization state for the photons at the inputs was one of the four entangled Bell states. The fidelity of teleportation is tied directly to the validity of this assertion, the strength of which depends critically on the absence of any way to distinguish the photons at the inputs to the beam splitter (save by their direction). The presence of any dispersive element in either path by which the two photons reach the inputs to the Bell apparatus can compromise such inductive inference, because it may provide a means by which the path taken by each photon to its detector can, in principle, be identified. This is sufficient to reduce the visibility of the HOM dip and the strength of any inductive inference based on it.

A nonclassical dispersion cancellation effect involving coincidence detection of entangled photon pairs was first analyzed by Franson [6]. A related effect in a HOM interferometer was subsequently demonstrated and analyzed by Steinberg *et al.* [7,8]. The experimental realization of this latter scheme used photon pairs generated via spontaneous parametric down-conversion (PDC) pumped by a monochromatic laser. Figure 1 provides a conceptual illustration of the dispersion cancellation that can occur in the HOM interferometer. The photons arriving at each detector may be labeled by their frequencies, and by their relative detection times. Any combination of observed frequencies and relative arrival

*Authors were at the Institute of Optics, University of Rochester, for this work.

†Author was at Department of Physics and Astronomy, University of Rochester, for this work.

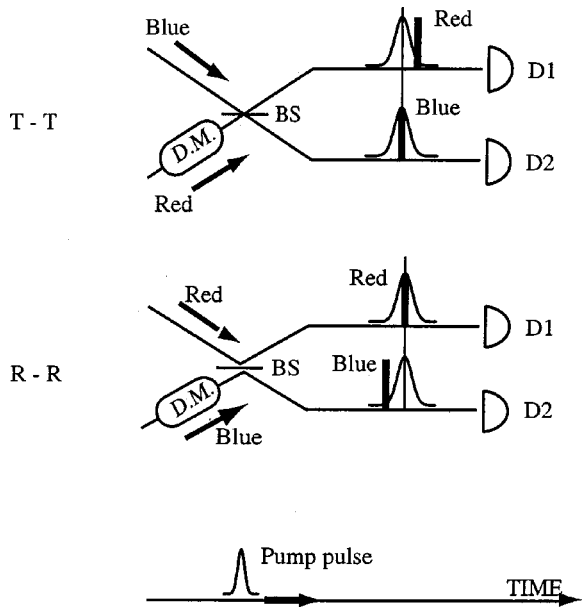

FIG. 1. The mechanism of dispersion cancellation. Two photons are incident on a beam splitter (BS), after one of them has passed through some dispersive material (D.M.) The photons have identical spectra, centered on the mean frequency ν_0, and the optical path lengths are balanced so that photons at this mean frequency arrive simultaneously at BS and at the detectors $D1$,$D2$. In the figure, a ''red'' photon with frequency $(\nu_0-\Delta\nu)$ is initially detected at $D1$, and a ''blue'' photon with frequency $(\nu_0+\Delta\nu)$ is subsequently detected at $D2$. There are two possible ways for this to occur: the first is that both photons were transmitted at the beam splitter $(T-T)$, and the second is that both were reflected $(R-R)$. The red and blue frequencies are oppositely shifted in velocity, as compared with the center of the photon wave packet (shown by the vertical line), so that the blue is delayed relative to the red by the same amount in each case. Therefore, the amplitudes for these two processes would interfere to completely suppress coincidences were it not for the presence of the classical (though unmeasured) pump pulse, which enables the *T-T* and *R-R* paths to be distinguished by their total transit times.

times could have come about in two distinct ways. For example, as depicted in the figure, a red photon might arrive first at the upper detector, followed by a blue photon at the lower detector (where ''red'' and ''blue'' refer to frequency shifts relative to the degenerate photon pair center frequency). This can occur either because both photons were transmitted at the beam splitter (*T-T*), or because both were reflected (*R-R*). In the *T-T* case, the red photon would have traveled through the dispersive material, while in the *R-R* case, the blue photon would have done so. Because the blue is delayed more than the red by the dispersive material, the total travel time for the photons is shorter for the *T-T* case than it is for the *R-R* case. However, in both cases, the blue photon is expected to arrive later than the red by the same amount of time, and so they are able to interfere destructively with complete visibility—just as a pair of degenerate-frequency photons would—and so the interference is unaffected by dispersion.

If the pump for the down-converter is continuous wave (cw), then the time at which the photon pair is generated is *a priori* unknowable—a fact that permits the interference of amplitudes for photon pairs created at different times. On the other hand, if the pump is an ultrashort optical pulse, then the time of generation of the photons may be known to much better precision than their correlation time, and in this case, the interference is compromised [9–11] because the *T-T* and *R-R* pathways then become distinguishable by virtue of their different transit times through the interferometer. The resulting loss of interference, and of dispersion cancellation, can also be understood in a frequency domain picture. In this picture, the frequency anticorrelation and entanglement necessary for these effects are reduced because the pump pulse is broad band, and offers a wide range of sum frequencies for the photon pairs that are not available in the cw-pumped case [9].

In practice, the interference can be restored at the expense of either timing information or count rate. In the past few years, some new nonlocality, entanglement swapping, and teleportation experiments have made use of interference from multiphoton sources [3,12]. An effective manner of achieving this involves synchronous pumping of several crystals with ultrashort pulses [13]. Lack of precise timing information from separate sources makes such experiments impossible because the photons sent to the Bell detector are more than likely in different temporal modes. They may nonetheless be mode matched by severe spectral filtering, but the associated reduction in the count rate makes experiments involving more than two detectors difficult.

In this paper we propose and analyze several means by which the interference visibility and dispersion cancellation in a HOM apparatus can be restored by suitable engineering of the source configuration—namely by tailoring the dispersive properties of the nonlinear crystal in which the down-converted pair is produced. At the same time, precise timing information about the photon pair is retained, so that such sources are likely to be of use in quantum communications schemes involving several independent sources of entangled photons, and in which long propagation paths for the entangled particles are necessary. One advantage of suppressing distinguishing information at the source is that higher count rates can be maintained, leading to more accurate measurements in experiments designed to test fundamental postulates, and higher data rates in quantum communications systems.

To do this we introduce a general framework for the analysis of all dispersive effects that arise in coincidence-counting experiments with parametric down-converters. Dispersion cancellation relies on two key ingredients: the frequency entanglement of the photon pair and the frequency-dependent time delay imparted to the photons by the dispersive material. These aspects of the problem lend themselves naturally to analysis in the frequency domain. A recent paper [14] has already presented a time-domain analysis of the effect of dispersion for the specific case of type-II PDC pumped by an ultrashort chirped pump pulse in a collinear HOM interferometer; here we generalize certain of those results. We consider both type-I and type-II crystal phase matching, and identify methods for each by which the distinguishing information introduced by external dispersion

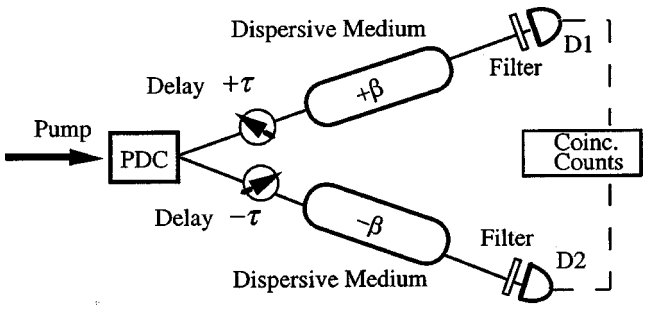

FIG. 2. Franson's noninterferometric configuration, in which photon pairs exhibit nonlocal cancellation of dispersive effects even though they are never spatially overlapped. A pump beam creates pairs of signal (*s*) and idler (*i*) photons in a parametric down-converter (PDC) that are sent to a pair of detectors ($D1$,$D2$) after passing through variable delay lines, dispersive media, and spectral filters. The delays ($\pm\tau$) are symmetric for computational convenience. The dispersive media in each arm are characterized by group-velocity dispersions $\pm\beta$; when these media have equal lengths, the effects of dispersion are canceled in the coincidence-counting profiles.

can be suppressed for a pulsed pump.

II. TWO TYPE-I PDC CONFIGURATIONS

We begin by describing in more detail the two cases in which dispersion cancellation effects were reported initially. Figure 2 shows the configuration analyzed by Franson [6]. Pump photons entering the crystal produce pairs of ''signal'' and ''idler'' photons, each of which pass through a different dispersive medium before being detected. Photon counters measure the coincidence rate as a function of the adjustable relative path delay that is installed in one or both arms. Classically, this measurement would show broadening of the intensity correlation peak regardless of the specific dispersive properties of the two elements. The quantum-mechanical treatment, however, reveals that if the elements have equal length, but group-velocity dispersion (GVD) of equal magnitude and opposite sign, the coincidence rate profile would remain largely unaffected—the dispersive broadening would be cancelled to the GVD level of approximation, due to the frequency entanglement of the photon pairs. Unfortunately, the temporal resolution of currently available photodetection systems does not seem to permit observation of this effect.

Later, Steinberg *et al.* [7,8] observed cancellation in a HOM interferometer with type-I PDC, in which a dispersive element was added to just one arm as in Fig. 3. Rather than a correlation peak, the coincidence rate as a function of the relative path delay in this configuration displays a background rate with a dip whose width corresponds to the photon wave-packets' overlap time. Experimental observation is possible in this case because the coincidence null is generated by an interference effect, so that a slow detector response does not limit the temporal resolution of the measurement. No reduction of visibility or broadening in the coincidence rate profile was observed in that experiment, even when the added element would have corresponded classically to an observable 60-fs broadening of the temporal

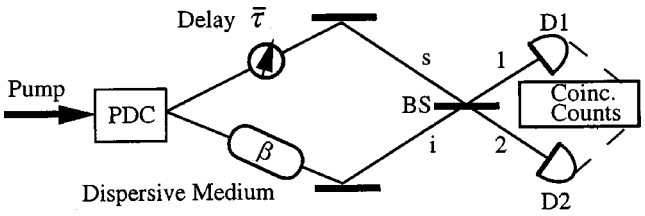

FIG. 3. A HOM interferometer with dispersive delay added to the lower arm. The pump beam (or pulse) creates signal (*s*) and idler (*i*) photons in the PDC that are later brought together at a beam splitter and counted in coincidence at detectors $D1$ and $D2$.

profile [8]. Although the second-order (GVD) dispersive terms canceled in their calculation, Steinberg *et al.* noted that higher, odd-order dispersive effects should in fact be enhanced—though again, these effects were too small to be observed. They also noted that in the special case of ''balanced dispersion,'' in which identical dispersive elements are in both paths of the interferometer, *all* dispersive effects will be cancelled.

These cancellation effects depend on the use of a cw pump. In Secs. III and IV we will examine the consequences when an ultrashort pump pulse is used instead. For computational clarity, we will discuss the two configurations in reverse historical order: in Sec. III we consider the HOM interferometer, and in Sec. IV, the noninterferometric configuration.

III. DISPERSION IN THE PULSED HOM INTERFEROMETER

A. Calculation of the coincidence-counting rate

We now consider the interferometer of Fig. 3, but with the cw pump beam replaced by a train of broad-band optical pulses. In our analysis, we will include the dispersive effects in the crystal source itself, with the objective of using these to influence, or possibly restore, dispersion cancellation and interference effects. The beam angle is assumed to be sufficiently small so that all transverse effects are neglected, and the center frequency of the photon pair is taken to be degenerate. A dispersive element is in the lower path, while the upper path has only a variable path delay. The pump field strength is assumed to be low enough so that on the order of one pair is generated per pass in the crystal, yet large enough to be treated as a classical coherent field in this calculation; only the spontaneously generated signal and idler fields are quantized. Following a first-order perturbation expansion of the interaction Hamiltonian, the resulting two-photon state [9] can then be given by

$$|\psi\rangle = K\int_0^\infty\int_0^\infty d\omega_s d\omega_i \alpha(\omega_s+\omega_i)\phi(\omega_s,\omega_i)|\omega_s\rangle_s|\omega_i\rangle_i \tag{1}$$

where $|\omega_m\rangle_n \equiv \hat{a}_n^\dagger(\omega_m)|0\rangle_n$ is a single photon state of frequency ω_m in mode *n*. This state is a sum over all possible (entangled) pairs of frequencies in the signal and idler modes, and can be used to describe either of the two types of down-conversions. For type-I PDC, the signal and idler

modes are distinguished by their directions of propagation, while in type-II PDC they are distinguished by polarization or propagation direction, or both. In either case, the directions of the emission to be detected can be defined by small, distant apertures, and are assumed to be sufficiently close to the propagation axis that transverse effects may be neglected. The spontaneous generation of these photon pairs from a pump photon is constrained by energy conservation, $\omega_p = \omega_s + \omega_i$ so that the pump's amplitude spectral profile may be written as $\alpha(\omega_s+\omega_i)$. The PDC crystal's spectral ''phase-matching function'' (PMF), or $\phi(\omega_s,\omega_i)$, is defined in Appendixes *A* (type-I) and *B* (type-II). It may be interpreted as giving the amplitude contribution for each frequency pair resulting from the PDC of a given pump frequency; meanwhile, the pump profile weights the availability of various pump frequencies for such pairs. *K* is a normalization constant:

$$K^{-2} \equiv \int_0^\infty \int_0^\infty d\omega_s d\omega_i |\alpha(\omega_s+\omega_i)|^2 |\phi(\omega_s,\omega_i)|^2 |\omega_s\rangle_s |\omega_i\rangle_i . \tag{2}$$

The rate of coincidence counts at time t_1 at detector 1 and t_2 at detector 2 with a coincidence-counting window of duration T is given by [15]

$$R \propto \int_0^T \int_0^T dt_1 dt_2 \langle \psi | \hat{E}_1^{(-)}(t_1) \hat{E}_2^{(-)}(t_2) \hat{E}_2^{(+)}(t_2) \hat{E}_1^{(+)}(t_1) | \psi \rangle, \tag{3}$$

where $\hat{E}_{1,2}^{(+)}$ are the positive-frequency electric field operators at detectors 1 and 2, and $\hat{E}_{1,2}^{(-)}$ are their Hermitian conjugates. Due to the action of a properly chosen (50-50) beam splitter, these field operators can be related to the signal and idler field operators by [15]

$$\hat{E}_1^{(+)} = \frac{1}{\sqrt{2}} (\hat{E}_s^{(+)} + \hat{E}_i^{(+)}),$$

$$\hat{E}_2^{(+)} = \frac{1}{\sqrt{2}} (\hat{E}_s^{(+)} - \hat{E}_i^{(+)}), \tag{4}$$

where

$$\hat{E}_s^{(+)}(t_s) = \int_0^\infty d\omega_s A(\omega_s) \hat{a}_s(\omega_s) e^{-i\omega_s(t_s-\tau)},$$

$$\hat{E}_i^{(+)}(t_i) = \int_0^\infty d\omega_i A(\omega_i) \hat{a}_i(\omega_i) e^{-i[\omega_i t_i + \kappa(\omega_i) l]} \tag{5}$$

contain the annihilation operators $\hat{a}_{s,i}$ for the signal and idler modes (labeled ''s'' and ''i'' in Fig. 3). The variable free-space delay τ is in the signal arm, while the dispersive medium of length l is in the idler arm. The dispersion relation $\kappa(\omega_i)$ gives the wave number of the light inside the dispersive medium so that a phase delay $\kappa(\omega_i)l$ is imparted to each frequency component of the idler photon wave packet. The $A(\omega_{s,i})$ contain dimensional factors so that $|\hat{E}_{s,i}|^2$ are in units of photons per second; they vary slowly with frequency and can be taken outside the integrals as constants. After inserting Eqs. (1), (4), and (5) into Eq. (3) and carrying out the integrals over time with the limits extended to infinity [9], we have

$$R(\tau) \propto \int_0^\infty \int_0^\infty d\omega_s d\omega_i |\alpha(\omega_s+\omega_i)|^2 \{ |\phi(\omega_s,\omega_i)|^2 - \phi(\omega_s,\omega_i)\phi^*(\omega_i,\omega_s) \times e^{i\{(\omega_s-\omega_i)\tau + [\kappa(\omega_s)-\kappa(\omega_i)]l\}} \}. \tag{6}$$

To proceed further, we require explicit functional forms for α and ϕ. As in [9], we will use a transform-limited Gaussian pump pulse, which results in a Gaussian frequency distribution centered at $2\overline{\omega}$ with a bandwidth parameter σ,

$$\alpha(\omega_s+\omega_i) = e^{-(\omega_s+\omega_i-2\overline{\omega})^2/2\sigma^2}. \tag{7}$$

Next we make the change of variables

$$\nu_{s,i} \equiv \omega_{s,i} - \overline{\omega}, \tag{8}$$

where $\overline{\omega}$ is the degenerate center frequency for signal and idler photons, and we extend the limits of integration for ν_s, ν_i to minus infinity.

We also wish to explicitly include the dispersive properties of the external medium; these are encoded in $\kappa(\omega)$, and can be brought to light via a Taylor-series expansion about $\overline{\omega}$. We have for the $[\kappa(\omega_s)-\kappa(\omega_i)]$ term,

$$\kappa(\nu_s)-\kappa(\nu_i) = \kappa + \kappa'(\nu_s-\nu_i) + \frac{1}{2}\kappa''(\nu_s^2-\nu_i^2) + \frac{1}{3!}\kappa'''(\nu_s^3-\nu_i^3) + \cdots, \tag{9}$$

where κ is the wave number evaluated at $\overline{\omega}$ and all derivatives are evaluated there as well. We adopt the notation for the group-velocity dispersion (GVD) in the external medium,

$$\beta = \frac{1}{2}\kappa'' = \frac{1}{2}\left.\frac{d^2\kappa(\omega)}{d\omega^2}\right|_{\omega=\overline{\omega}} \tag{10}$$

and discard terms of higher order than this in the calculation. Using the inverse group velocity κ', we can offset the free-space photon delay by the mean transit time through the external dispersive medium of length l to get the true relative photon delay at the beam splitter,

$$\overline{\tau} \equiv \frac{1}{\sqrt{2}}(\tau - \kappa' l). \tag{11}$$

The scale factor of $1/\sqrt{2}$ is added for later convenience. Rewriting Eq. (6) with these substitutions, we arrive at the general expression for the coincidence-counting rate in a pulsed HOM interferometer with external dispersion:

$$R(\bar{\tau},\beta)=K_1\int_{-\infty}^{\infty}\int_{-\infty}^{\infty}d\nu_s d\nu_i e^{-[(\nu_s+\nu_i)/\sigma]^2}\times\{|\phi(\nu_s,\nu_i)|^2-\phi^*(\nu_i,\nu_s)\phi(\nu_s,\nu_i)\times e^{i[(\nu_s-\nu_i)\bar{\tau}+\beta l(\nu_s^2-\nu_i^2)+(1/3!)\kappa''' l(\nu_s^3-\nu_i^3)]}\}. \quad (12)$$

Here K_1 is a constant of proportionality that is the product of the photon detection and collection efficiencies, the pulse repetition rate, the pair-creation efficiency of the PDC crystal, the fourth power of the dimensional constant A in Eq. (5), and the square of the normalization constant K defined in Eq. (2).

B. Type-I HOM interference

Upon inserting into Eq. (12) the phase-matching function ϕ from Eq. (A12) we have, for type-I HOM interference,

$$R^I(\bar{\tau},\beta)=K_1\int_{-\infty}^{\infty}\int_{-\infty}^{\infty}d\nu_+ d\nu_- e^{-(\nu_+/\sigma)^2}\times\mathrm{sinc}^2[(t_+\nu_+ + BL\nu_-^2+\bar{B}L\nu_+^2)/2]\times[1-e^{2i(\bar{\tau}\nu_- +\beta l\nu_+\nu_-)}], \quad (13)$$

where $\mathrm{sinc}(x)\equiv(1/x)\sin(x)$, $t_\pm$, B, $\bar{B}$ are defined in Eqs. (A9)–(A11), and

$$\nu_\pm=\frac{1}{\sqrt{2}}(\nu_s\pm\nu_i). \quad (14)$$

The PDC crystal has length L, while B, $\bar{B}$ are its second-order dispersive parameters. The constant background term in Eq. (13) is

$$C\equiv K_1\int_{-\infty}^{\infty}\int_{-\infty}^{\infty}d\nu_+ d\nu_- e^{-(\nu_+/\sigma)^2}\times\mathrm{sinc}^2[(t_+\nu_+ + BL\nu_-^2+\bar{B}L\nu_+^2)/2]. \quad (15)$$

This term represents the coincidence rate for large values of $\bar{\tau}$, outside the HOM dip; in this region, where interference does not occur, half of the photon pairs that reach the beam splitter will leave it in opposite directions (T-T and R-R events) and may go on to produce coincidence counts. We will normalize our coincidence-counting rates so that this background rate has a value of ''1'' in all of our plots.

To carry out the remaining integral in Eq. (13) we may use the identity

$$\mathrm{sinc}^2(x)=\frac{1}{4}\int_{-1}^{1}\int_{-1}^{1}dz_1 dz_2 e^{i(z_1+z_2)x}. \quad (16)$$

After using the coordinate transformations,

$$y=\tfrac{1}{2}(z_1-z_2),\qquad z=\tfrac{1}{2}(z_1+z_2), \quad (17)$$

the integrand in Eq. (16) is independent of y, so that

$$\mathrm{sinc}^2(x)=\int_{-1}^{1}dz\int_{-(1-|z|)}^{(1-|z|)}dy\, e^{i2zx}=2\int_{-1}^{1}dz(1-|z|)e^{i2zx}. \quad (18)$$

After the sinc^2 term in Eq. (13) is rewritten in this form, the integrals over ν_+ and ν_- can be carried out analytically. The result is then divided by C to obtain the normalized type-I coincidence-counting rate:

$$R_n^I(\bar{\tau},\beta)=1-\frac{1}{C}\int_{-1}^{1}dz\frac{(1-|z|)\Omega_z}{\sqrt{(\Omega_z\beta l)^2-iBLz}}\times\exp\left[\frac{-\left(\bar{\tau}-\frac{1}{2}t_+\Omega_z^2\beta l z\right)^2}{(\Omega_z\beta l)^2-iBLz}\right]\exp[-(\tfrac{1}{2}\Omega_z t_+ z)^2], \quad (19)$$

where Ω_z is defined by

$$\frac{1}{\Omega_z^2}=\frac{1}{\sigma^2}-i\bar{B}z. \quad (20)$$

The $\bar{B}$ term's contribution is relatively small for typical pump bandwidths, so that Ω_z is essentially σ, the pump bandwidth. The expression in Eq. (19) involves the dispersive parameters of the PDC crystal (k',k_p',k'',k_p'') through the B and $\bar{B}$ terms in the phase-matching function, while the external media dispersion (β) enters via phase terms in the electric-field operators. The latter terms are the ones subject to the cancellation effects.

The integral in Eq. (19) can be evaluated numerically. Figure 4 shows a plot of the normalized counting rate R_n as a function of delay $\bar{\tau}$ and external dispersion βl for a typical pulsed down-conversion arrangement: the crystal parameters k'' and t_+ (see Appendix A), were chosen to correspond to 1-mm-thick beta barium borate (BBO) [16], and the pump pulse duration was taken to be 100 fs. The plot shows that for a pulsed pump, the degree of interference is reduced as the magnitude of introduced dispersion is increased. This reduction starts being discernible already for dispersion values of $\beta l=2\times10^{-4}\,\mathrm{ps}^2$, which corresponds to a block of BK-7 glass with a length of 1 cm. The plot also shows that external dispersion affects the visibility of the interference dip more dramatically than it affects the width.

For a fixed nonzero value of external dispersion, the interference visibility is reduced as the pump pulse is shortened (Fig. 5) and in the extreme limit of an infinitely broad-band pump, the interference vanishes altogether. In the temporal domain, this limit corresponds to precise knowledge of the pair creation time, which is constrained by the pump pulse duration (see Fig. 1). Alternatively, in the frequency domain, the interference reduction is associated with decorrelation of the pair frequencies by the broad-band pump pulse.

Figure 5 shows that the count profile with respect to delay $\bar{\tau}$ is in general asymmetric about the origin in the presence of

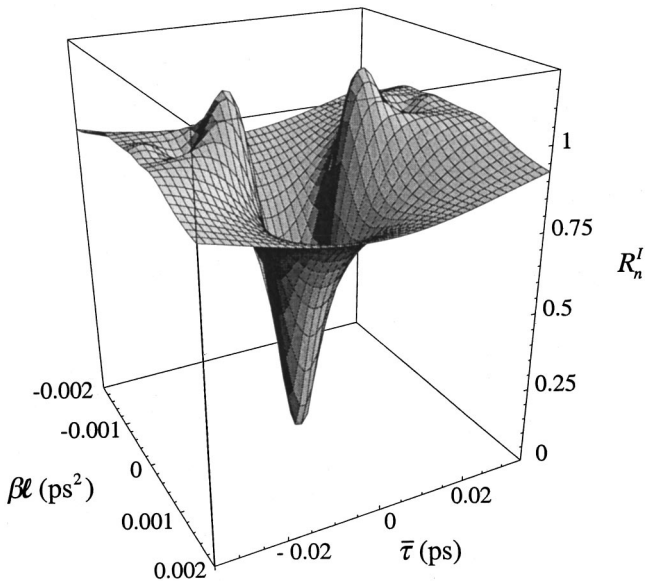

FIG. 4. Normalized coincidence counting rate R_n^I in a HOM interferometer with a pulsed type-I source, as a function of relative photon delay $\overline{\tau}$ and external dispersion βl. The interference visibility is complete at zero delay ($\overline{\tau}=0$) when no external dispersion is introduced ($\beta l=0$). As the dispersion in the path medium is increased, interference is reduced, so the dispersion cancellation common to the cw-pumped situation does not occur here. Note that the 10-fs width of this interference dip is an order of magnitude narrower than that produced by the same length of crystal in type-II PDC [10]. The plot was made using Eq. (19) with a pump bandwidth of $\sigma=30\times10^{12}\,\mathrm{rad}^{-1}$ (for 100-fs duration at 810 nm), and PDC parameters corresponding to 1 mm of BBO: $t_+=-0.05$ ps and $BL=3.65\times10^{-5}$ ps^2.

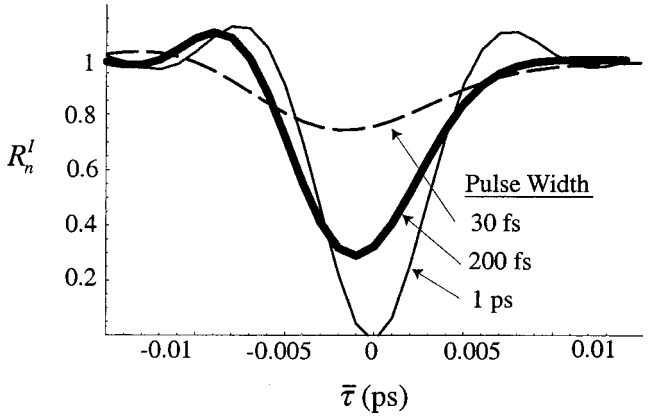

FIG. 5. Type-I HOM interference dips for three different pump pulse widths. For the longest pump pulse (1 ps), the dip is identical to that produced by a cw pump—symmetrically-shaped and having full visibility. For the 200-fs pump pulse, the dip exhibits asymmetry, reduced visibility, and a shift in the minimum away from $\overline{\tau}=0$. For the shortest pump pulse (30 fs), the effects of the previous case become even more pronounced, and interference is virtually eliminated. Plots were made using Eq. (19). The external dispersion was fixed at $\beta l=2.5\times10^{-4}$ ps^2, which corresponds to 1.25 cm of BK-7 glass. For the PDC crystal, $BL=3.65\times10^{-5}$ ps^2 and $t_+=-0.05$ ps (appropriate to 1 mm of BBO).

external dispersion. This is physically due to the fact that for any given frequency pair, the dispersive constant β in Eq. (13) produces a phase delay of fixed sign, whereas the time delay phase term $\overline{\tau}\nu_-$ changes sign at the origin. Hence the total accumulated phase over all the detection frequencies is not symmetric for positive and negative values of $\overline{\tau}$, and therefore, neither is the coincidence profile. Exceptions to this are the cases where t_+ is zero (the pump photon has the same group velocity as the signal photons), or where β is zero (no external dispersive medium is present); in these cases, the count profile is symmetric for any value of the PDC crystal dispersion, as seen in Fig. 4 along the line $\beta l=0$.

C. Tailoring of a type-I crystal to recover lost interference

We will now examine possible methods of minimizing the effects of the unbalanced external dispersion. The features of prime interest are the interference visibility and the range of delays $\overline{\tau}$ over which it is maintained. For some applications, an interference dip that is very narrow in $\overline{\tau}$ is advantageous [8], while in others [3,12,13] it is desirable to maximize the interference over a large range of photon delays. We therefore seek methods of tailoring the source to address both of these requirements.

Equation (13) suggests two possible ways in which the effects of external dispersion might be minimized, or eliminated altogether. The term which represents external dispersion, βl, is multiplied by both integration variables—the down-conversion frequency sum ν_+ and difference ν_-. If either of these variables could be made zero, or restricted to a small range, then the contribution of this term to the integral could be made negligible.[1] The sinc^2 function in Eq. (13), which has both ν_+ and ν_- as its arguments, presents a way of achieving this: for in the long-crystal limit, the sinc^2 function can be made to approach $\delta(\nu_+)$ or $\delta(\nu_-)$ with suitable choices for the dispersive parameters of the crystal. Both possibilities are suggested by Eq. (13); they will now be investigated using the full calculation given by Eq. (19).

Method 1: Restrict the values of ν_-

If t_+ and $\overline{B}$ are made small, while BL is made large, the phase-matching term in Eq. (13) approaches the limiting form

$$\lim_{L\to\infty}[\mathrm{sinc}^2(BL\,\nu_-^2/2)]\propto\delta(\nu_-). \tag{21}$$

BL can be made large most easily by choosing a long crystal. The condition $t\cong0$ requires that $k_p'\cong k'$, and $\overline{B}L$ (whose effects are already small due to the pump profile) would be small if $k_p''\cong\frac{1}{2}k''$. Under these conditions, the phase-matching function is aligned with the $\nu_s=\nu_i$ axis,

[1]In fact, this is how spectral filters mitigate the effects of external dispersion, though they accomplish this by restricting the signal and idler frequencies independently, and not just their sums or differences. See Appendix C, case 3.

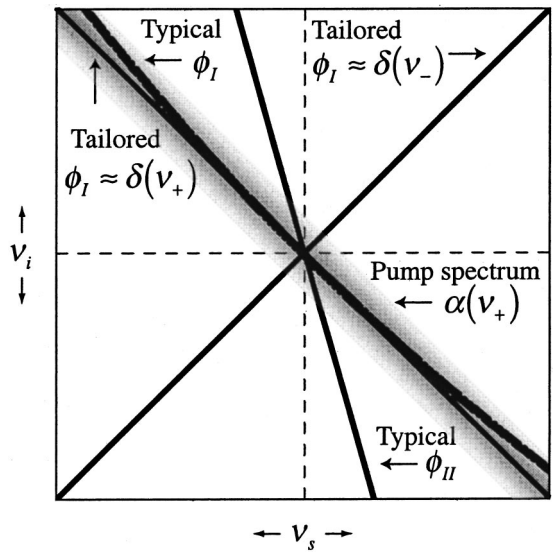

FIG. 6. Examples of phase-matching functions and a pump pulse spectrum as functions of the signal and idler frequencies in the long crystal limit. The pump spectrum $\alpha \propto e^{-(\nu_s+\nu_i)^2}$ is depicted as a gray band along the line $\nu_s=-\nu_i$; the shading represents the Gaussian distribution of sum-frequency values. If the pump were cw, this band would have zero width. The line labeled ϕ_{II} is a general type-II PMF, which behaves as $\phi_{\mathrm{II}} \approx \delta(a\nu_s + b\nu_i)$ to first order in the signal and idler frequencies, and is not symmetric in the signal and idler frequencies it allows. A tailored type-I PMF, $\phi_{\mathrm{I}} \approx \delta(\nu_-)$, lies along the line $\nu_s=\nu_i$, and a general type-I PMF, which behaves as $\phi_{\mathrm{I}} \approx \delta(c\nu_+ + d\nu_-^2 + e\nu_+^2)$ to second order, is also shown. For each source of photons, down-converted pairs are produced in the intersection of the pump spectrum and the appropriate PMF; in each case, the ranges of allowed frequencies, and their correlations, can dramatically alter the HOM interference visibility and dispersion cancellation.

when plotted as a function of ν_s and ν_i (see Fig. 6). This indicates a high-frequency correlation for the down-converted photons ($\nu_s=\nu_i$) in the long crystal limit.

The implication of this δ-function limit and the associated condition, $\nu_-=0$, is that the dispersive β terms in Eq. (12) are eliminated, in apparent analogy with the cw-pumped case (see Appendix C, case 2). But in contrast to that case, here all orders of external dispersion in $\kappa(\omega_{s,i})$, both even and odd, are eliminated as can be seen from Eq. (9). This is because the frequency pair variables are now directly correlated, rather than anti-correlated as in the cw-pumped case.

Figure 7 shows the improved HOM visibility that results. The normalized coincidence rate is plotted as a function of delay for a typical source and for idealized sources tailored according to this method (and a second method described below). Note that the $\phi_I \approx \delta(\nu_-)$ source produces destructive interference that is not only complete, but also present over a much broader range of photon delays than for the typical type-I source. This is because the frequency difference phase term $\bar{\tau}\nu_-$ in Eq. (13), containing the relative two-photon time delay, is also suppressed by $\delta(\nu_-)$, and would vanish altogether in the limit $\nu_- \to 0$. The result is a large increase in the width of the restored interference null and in the limiting case, a null of infinite width in $\bar{\tau}$. In other

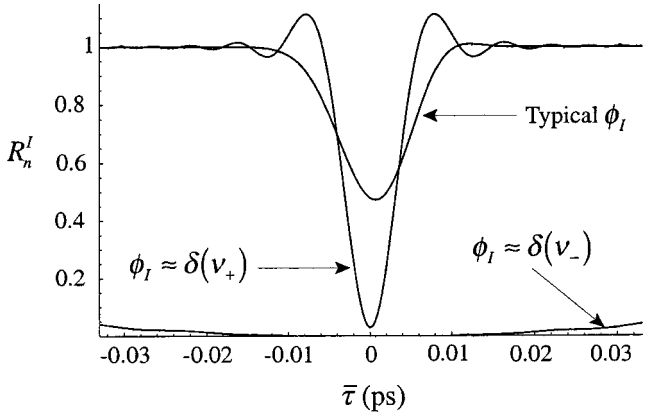

FIG. 7. Restored HOM interference from a tailored type-I crystal. A typical normalized coincidence rate R_n^I is shown for a 1-mm-long BBO down-converter pumped by a 100-fs pulse, with 5 mm of dispersive glass in one of the photon paths. The case $\phi_{\mathrm{I}}=\delta(\nu_-)$ for method 1 was modeled as a crystal having very large B (100 times that of BBO) while retaining the $\bar{B}$, t_+, and L values for 1 mm of BBO. The interference is restored, and there is large temporal broadening of the dip. For method 2, $\bar{B}$ is very large (100 times that of BBO), while B, t_+, and L retain the values for 1 mm of BBO, so that $\phi_{\mathrm{I}} \approx \delta(\nu_+)$. Interference is again restored, while the dip width is essentially unchanged. Plots were made using Eq. (19).

words, photon pair members generated in the limiting case would always be incident on the same detector, with identical frequencies, no matter what relative delays were imposed on them before their arrival at the beam splitter.

We emphasize that this is a nonclassical interference effect, which arises from a new kind of entanglement for down-converted photons. Our tailored source in this case constrains the frequency difference for the photon pair, without constraining the frequencies themselves—that is, the photon frequencies are highly correlated, even though it can be verified that each individual photon has a broad spectrum [9]. This is in contrast to the entanglement created by cw pumping (in which the frequency sum is constrained), and is also different from the restoration of interference with spectral filters (in which no entanglement is present at all). While it is true that narrow-band spectral filters could reproduce the broad temporal interference profile of Fig. 7, they would do so by increasing the duration of each photon's wave packet independently; this differs from the present method, in which the signal and idler photons retain short temporal durations. We refer the reader to Appendix C for details on the effects of cw pumping and narrow-band filters.

Method 2: Restrict the value of ν_+

Now we return to Eq. (13) and, instead of making $\bar{B}$ negligible, we choose it to be large, so that the term $\bar{B}\nu_+^2$ dominates the argument of the sinc^2 function. In the long crystal limit, this produces the δ function

$$\lim_{L\to\infty} [\mathrm{sinc}^2(\bar{B}L\nu_+^2/2)] \propto \delta(\nu_+). \tag{22}$$

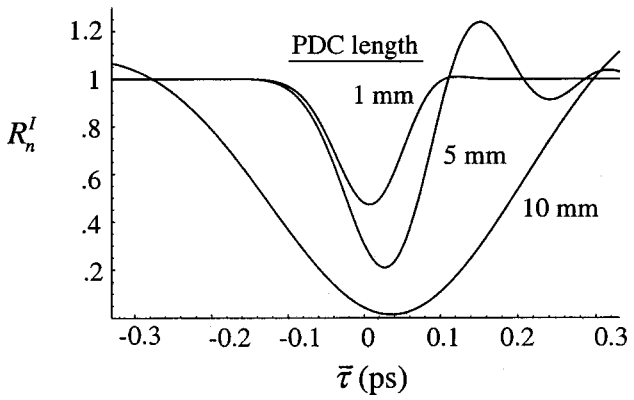

FIG. 8. The effect of a long PDC crystal on type-I HOM interference. Even without special tailoring, for type-I PDC, a sufficiently long crystal (BBO in this case) restores interference that was reduced to 50% by a 100-fs pump pulse and external dispersion due to 5 mm of glass. The degree of asymmetry in $\bar{\tau}$ depends on the magnitude of the product of Ω, β, and t_+ in Eq. (19).

In this case the dispersive βl term in Eq. (13) is again eliminated, but now the phase term $\bar{\tau}\nu_-$ is not, so that we expect no temporal broadening of the count profile (in contrast to the previous method.) The plot for $\phi_I \approx \delta(\nu_+)$ in Fig. 7 confirms that this is indeed the case, and that the visibility can be fully restored with a narrow dip. Also, the orientation of the PMF for this case, shown in Fig. 6, matches that of the pump profile (along $\nu_s = -\nu_i$) and would therefore produce even-ordered cancellation effects similar to those observed with a cw pump (see Appendix C, case 2).

An increase in $\bar{B}$ while keeping B small corresponds physically to a large GVD for the pump pulse but a very low GVD for the signal and idler photons. This implies that for this particular tailoring method, some classical timing information will be lost due to dispersive broadening of the pump pulse. For example, after propagation through a PDC crystal of length $L=1$ cm with an unusually high pump dispersion ($\bar{B}=2\times10^{-6}\,\mathrm{ps}^2/\mu\mathrm{m}$, ten times larger than a typical value), a 100-fs pulse $\sigma=30\,\mathrm{ps}^{-1}$ will be stretched to become approximately $\sigma\bar{B}L=1$ ps in duration [17]. This effect does not occur with the previous tailoring method.

Both of the above methods involve a long down-conversion crystal, and even if no special dispersive properties are chosen, it is possible to have both effects at work in the same source. Each effect serves to increase the dip visibility in the presence of external dispersion, but the first effect is accompanied by a broadening of the temporal width of the dip, while the second is not. In fact, as shown in Fig. 8, a typical type-I crystal of sufficient length will have the effect of restoring the visibility (this is not true for the type-II case—see Sec. III E). Apparently, the minimum magnitude of the crystal's dispersive phase BL required to restore full interference visibility is on the same order as the external dispersive phase βl. From Fig. 8 we also see that for broadening of the dip with respect to $\bar{\tau}$, approximately 10 cm of a typical PDC crystal would be required to establish very high interference visibility over a relative delay range of about 10 fs.

Finally, we wish to comment on a third approach that appears to follow from Eq. (12), namely, the elimination of all second-order terms in the sinc^2 argument to create a PMF of the form $\phi_I \approx \delta(t_+\nu_+)$. Such a first-order truncation of the type-I phase-matching function seems plausible, but leads to inconsistencies when the full calculation is carried out using Eq. (18). The difficulties arise because no first-order ν_- term is present in the type-I expansion of ΔK (see Appendix A).

D. Type-II HOM interference

The type-II phase-matching function ϕ_{II}, given by Eq. (B3), can also be inserted into the master equation (12) to yield

$$R^{\mathrm{II}}(\bar{\tau},\beta) \propto \int_{-\infty}^{\infty}\int_{-\infty}^{\infty} d\nu_+ d\nu_- e^{-(\nu_+/\sigma)^2}\{\mathrm{sinc}^2[(t_+\nu_+ + t_-\nu_-)/2] - \mathrm{sinc}[(t_+\nu_+ + t_-\nu_-)/2]\mathrm{sinc}[(t_+\nu_+ - t_-\nu_-)/2] \times e^{2i(\bar{\tau}\nu_- + \beta l \nu_+\nu_-)}\}. \quad (23)$$

This can be integrated numerically as for the type-I case, after following steps analogous to Eqs. (13)–(19). Such a calculation is essentially a frequency-domain version of the one presented by Perina *et al.* [14], although here we choose to include only the (dominant) first-order dispersive terms in the PMF, while Perina *et al.* retained terms up to second order. (Second-order terms were also retained in the preceding section, where they were important because the signal and idler have the same index of refraction in type-I PDC). Also, the relative delay in Ref. [14] was imposed by a pair of quartz wedges that added dispersive material with increasing delay, whereas the $\bar{\tau}$ in our calculations is a free-space delay with an offset.

E. Tailoring a type-II crystal to recover interference

Method: Restrict the values of ν_-

The first thing to note from Eq. (23) is that, even in the absence of external dispersion, interference visibility is typically lost when type-II crystals are pumped by an ultrafast source, because $\phi_{\mathrm{II}}(\omega_o,\omega_e)$ is not symmetric under interchange of ω_o and ω_e [9]. However, an exception to this asymmetry has already been pointed out [10] when the condition $t_+=0$ is met: this corresponds to matching the group velocity of the pump pulse to the average group velocity of the down-conversion within the PDC. In that case, perfect visibility would be expected for a pulsed pump were it not for the presence of external dispersion.

Fortunately, just as for the type-I case we can see from Eq. (23) that if this condition is met, and if the crystal is made long enough, the PMF becomes

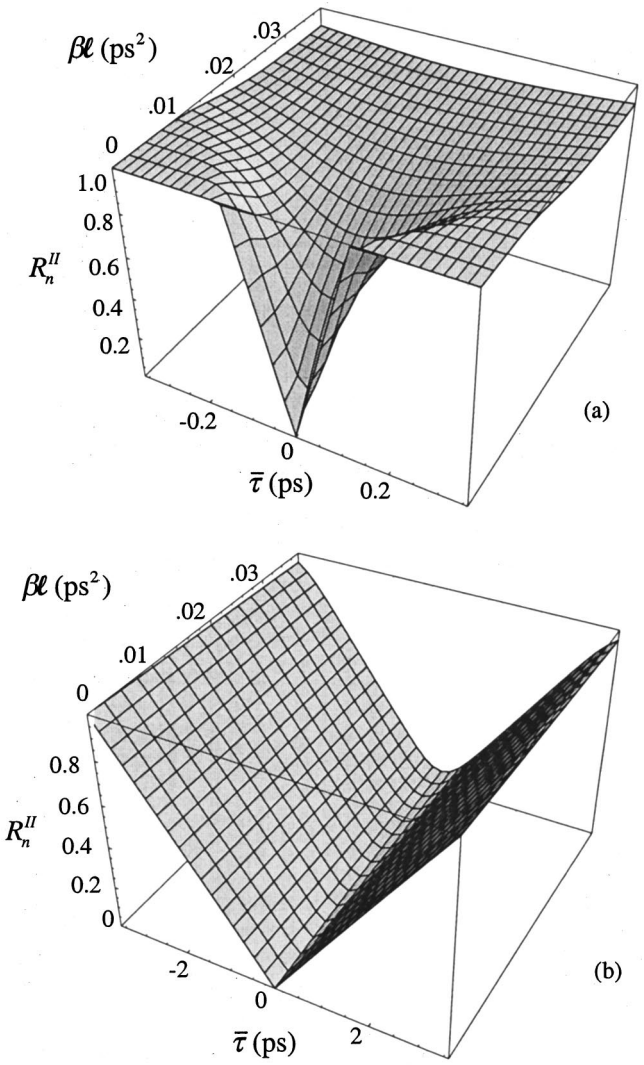

FIG. 9. The loss and restoration of type-II HOM interference with a 100-fs pulsed pump. The normalized coincidence-counting rate R_n^{II} is plotted as function of relative photon delay $\bar{\tau}$ and external dispersion βl. (a) For a 1-mm-long BBO source, interference visibility is lost as the external dispersion is increased. But it can be regained (b) with a long enough source crystal (10-cm BBO) whose PMF is tailored to lie exactly along the $\nu_s=\nu_i$ axis (see Fig. 6). Without the tailored PMF, no interference at all would be observed with such a long crystal.

$$\lim_{L\to\infty}\{\phi_{\mathrm{II}}(\nu_0,\nu_e)|_{t_+=0}\}$$
$$=\lim_{L\to\infty}\{\mathrm{sinc}[(t_+\nu_+ + t_-\nu_-)/2]|_{t_+=0}\}$$
$$=\lim_{L\to\infty}\{\mathrm{sinc}(t_-\nu_-/2)\}\propto\delta(\nu_-). \qquad (24)$$

The result is in effect the same as that obtained by the first tailoring method for type-I PDC, with $\nu_-=0$ imposed in Eq. (13): dispersion is again canceled to all orders, and the dip is widened considerably. Figure 9(a) illustrates the interference lost from external dispersion under normal conditions, and Fig. 9(b) shows that it is restored by such a tailored, long crystal.

The constraint cited here, $t_+=0$, is simpler than the analogous one for type-I PDC ($t_+=\bar{B}=0$), because our type-II analysis retains only the first-order terms in ΔK (see Appendix B). The other condition, $t_-=0$, is of course precluded for this case, because the photons must possess distinct group velocities in type-II PDC.

Finally, we note that unlike the type-I case, the use of a very long crystal in type-II PDC without the constraint $t_+=0$ would result in the loss of all observable interference (because of the asymmetry in the PMF) as has already been shown [9].

F. Practical issues

Though the issues discussed above are of theoretical interest, we also wish to consider a few aspects related to the possible implementation of our methods. First, there is a subtle point concerning the use of long crystals as parametric down-converters: the state vector in Eq. (1) is an approximation that relies on the negligible probability of more than one down-conversion event occurring within a single pump pulse. For most applications of spontaneous PDC, and particularly for quantum computing and quantum cryptography, this is in fact a requirement. With typical pump sources (cw Ar^+ lasers, doubled Ti sapphire lasers, etc.) and PDC crystals (1 cm or less of BBO, $LiIO_3$, KDP, or KD*P) this turns out to be an excellent approximation. But if exceptionally long crystals are used, it is possible that the pump power would have to be reduced in order to remain in the single-pair regime.

Another practical concern for long crystals is the well-known problem of walk-off. If noncritical phase matching (to zero order) were available, then there would be no lateral walk-off of the pump beam from the signal and idler beams. However, the crystals suitable for these applications generally require angle tuning, which does entail such walk-off; this limits the effective crystal lengths for the down conversion. Compensating techniques involving alternating thin-layered assemblies, though laborious, could provide one partial solution to this problem. Also, much recent progress has been made in various types of ''quasi-phase-matching'' methods in both bulk and waveguide form. Certain nonlinear parameters may be effectively synthesized to achieve phase matching by means of domain control, and guided confinement could eliminate lateral walk-off. However, it is certainly not clear that all of the key parameters could be controled by these methods.

As for tailoring the dispersive parameters themselves, in general we expect it will be difficult to find nonlinear crystals with the specific properties listed here. For example, implementation of method 2 for type-I phase matching (Sec. III C) implies finding a large GVD for the pump pulse but a relatively low GVD at the signal and idler wavelengths, all within the same material. However, we note that in the case of type-II PDC, the requisite first-order symmetry condition $t_+=0$ has been identified [10] in natural crystals of BBO at a signal wavelength of 1.5 μm, and KDP at 1.08 μm. The former is compatible with common fiber transmission windows; however, conventional photon counters work best at

close to half that wavelength. In the case of type-I PDC methods, the ideal properties are not available in known natural crystals, but can be approached more closely in some than others. The limited selection of nonlinear materials, natural, assembled, or quasi-phase-matched will always pose restrictions on the dispersive properties. But regardless of which material properties do become available, the calculations presented here will allow quantitative evaluation of the various parameter tradeoffs, so that dispersive effects can be optimized in the absence of perfect solutions.

IV. DISPERSION IN THE PULSED NONINTERFEROMETRIC ARRANGEMENT

A. Preliminary remarks

The simplicity of Franson's configuration in Fig. 2 is that it highlights quantum-mechanical dispersion cancellation effects without the interference created by a beam splitter. In this arrangement, the two-photon detection amplitudes interfere nonlocally even though they never overlap after exiting the PDC crystal. The methods of Sec. III require a few modifications in order to examine the pulsed pump version of this fundamentally interesting arrangement.

In keeping with the original treatment [6], we will allow the detected frequency dependence to be controled by bandpass filters in front of the detectors rather than by the bandwidth of the phase matching as in the previous sections. Physically, this means that the spectral width of the filters is much narrower than that of the photon pair emitted by the crystal, which is often the case in practice. This approach also serves to illustrate in some detail the role played by the filter's spectral width in such configurations.

There is also no longer any need to integrate over the detector/counter system response time. In the previous configurations, interference produced a dip in the coincidence rate. The results were not affected by an increase in integration period beyond the dip width, so the time limits could be extended without limit, simulating the use of slow detectors. But in this noninterferometric case, the result is an intensity correlation peak whose observed width is limited by the detector response time (typically greater than 1 ns). Thus, detectors with a very fast response, compared with the photons' overlap time, are ideal for this application—whereas such fast detectors would actually generate no coincidence counts at all in the interferometric case [7]. Although a slow detector response is advantageous in a HOM interferometer for revealing interference, here it would actually mask the temporal effects.

B. Calculation of the coincidence-counting rate

The joint rate of photodetections for a signal photon at detector $D1$ at time t_s and an idler photon at detector $D2$ at time t_i, as depicted in Fig. 2, is

$$R(t_s,t_i,\tau)\propto\langle\psi|\hat{E}_i^{(-)}(t_i-\tau)\hat{E}_s^{(-)}(t_s+\tau)\hat{E}_s^{(+)}(t_s+\tau)\times\hat{E}_i^{(+)}(t_i-\tau)|\psi\rangle. \tag{25}$$

The free-space photon delays are written as $\pm\tau$ for computational convenience. The calculation is carried out using the filtered electric field operators given below

$$\hat{E}_i^{(+)}(l_i,t_i)=A\int_0^\infty d\omega_i e^{-[(\omega_i-\overline{\omega})/\sigma_F]^2}\hat{a}_i(\omega_i)\times e^{-i\omega_i(t_i-\tau)+k(\omega_i)l_i},$$

$$\hat{E}_s^{(+)}(l_s,t_s)=A\int_0^\infty d\omega_s e^{-[(\omega_s-\overline{\omega})/\sigma_F]^2}\hat{a}_s(\omega_s)\times e^{-i\omega_s(t_s+\tau)+k(\omega_s)l_s}, \tag{26}$$

where l_s, l_i are the lengths of dispersive media in the signal and idler paths. Here Gaussian spectral filter functions, centered at the degenerate down-conversion frequency $\overline{\omega}$, have been inserted in the operators to simulate band-pass filters before the detectors. The implicit assumption is that their bandwidth σ_F is much less than that of the light produced in the PDC crystal. Because of this, ϕ can be ignored in the state vector for the down-converted light in Eq. (1), so that the field operators at the detector acting on the state give

$$\hat{E}_i^{(+)}(l_i,t_i)\hat{E}_s^{(+)}(l_s,t_s)|\psi\rangle \propto\int_0^\infty\int_0^\infty d\omega_s\omega_i\alpha(\omega_s,\omega_i)\times e^{-[(\omega_s-\overline{\omega})/\sigma_F]^2}e^{-[(\omega_i-\overline{\omega})/\sigma_F]^2}\times e^{-i\omega_s(t_s+\tau)+\kappa(\omega_s)l_s}e^{-i\omega_i(t_i-\tau)+\kappa(\omega_i)l_i}|0\rangle. \tag{27}$$

Rather than solve the general case, we will focus here on the arrangement in which dispersive effects are known to be canceled for a cw pump: the two media are taken to have identical lengths ($l_s=l_i=l$) and GVD constants of equal magnitude but opposite sign ($\pm\beta$). In this case, the effects of GVD on the coincidence profile are canceled due to quantum interference [6].

As before, the calculation for the pulsed pump case proceeds by expanding to second order the propagation vectors in the external media:

$$\kappa(\omega_s)+\kappa(\omega_i)\cong(\kappa_0+\kappa'\nu_s+\tfrac{1}{2}\kappa''\nu_s^2)+(\kappa_0+\kappa'\nu_i-\tfrac{1}{2}\kappa''\nu_i^2)=2\kappa_0+\kappa'(\nu_s+\nu_i)+\beta(\nu_s^2-\nu_i^2). \tag{28}$$

The origins for the time axes in Eq. (27) can be chosen so that $t_s=t_i=0$, yielding

$$\hat{E}_i^{(+)}\hat{E}_s^{(+)}|\psi\rangle \propto\sigma\sigma_F\int_{-\infty}^\infty\int_{-\infty}^\infty d\nu_s d\nu_i e^{-[(\nu_s+\nu_i)^2/2\sigma^2]}e^{-[(\nu_s^2+\nu_i^2)/\sigma_F^2]}\times e^{i[\tau(\nu_s-\nu_i)+\kappa' l(\nu_s+\nu_i)+\beta l(\nu_s^2+\nu_i^2)]}|0\rangle. \tag{29}$$

The first-order dispersion factor κ' is the inverse of the photon's group velocity in the external media. Noncontributing phase factors accumulated outside the integral do not affect

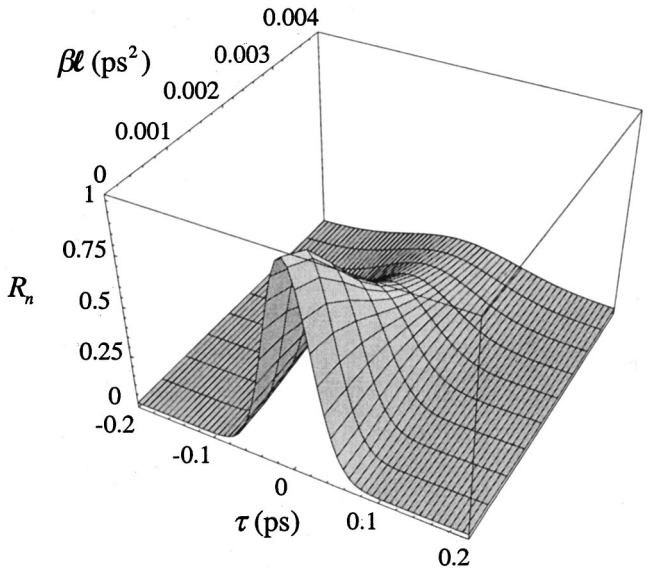

FIG. 10. The normalized two-photon counting rate R_n in the Franson configuration with a pulsed pump as a function of relative delay τ between the photon arrival times. As the external dispersion βl is increased, the peak decreases and broadens, exhibiting a loss of dispersion cancellation. The plot was made using Eq. (30) with $k'=0$. The pump and filter bandwidths were both set at $\sigma=\sigma_F=8\times10^{12}\,\mathrm{rad}^{-1}$ (the latter corresponds to a 40-nm band-pass filter centered at 800 nm for the photon pair).

the results and can be suppressed. Inserting Eq. (29) into Eq. (25) and carrying out the integrals yields

$$R(\tau)\propto\frac{(\sigma\sigma_F)^2}{1+(\sigma/\sigma_F)^2+(\beta l\sigma\sigma_F)^2}\times\exp\left[\frac{-\tau^2(\sigma^2+\sigma_F^2)-(\kappa' l\sigma)^2}{1+(\sigma/\sigma_F)^2+(\beta l\sigma\sigma_F)^2}\right] \tag{30}$$

for the probability of a coincidence count as a function of relative photon delay τ. A normalized version of this, R_n, is plotted in Fig. 10; the profile is a positive correlation peak in τ whose width depends on the pump bandwidth σ and the filter bandwidths σ_F. The figure demonstrates that the external dispersion broadens the count profile and reduces its peak value. Once again, a broad-band pump and dispersive media serve to reduce the dispersion cancellation effects.

Some interesting limiting cases of Eq. (30) are presented in Appendix D. As before, the cw-pumped limit can be investigated by replacing the pump spectrum in Eq. (29) with a δ function, so that $\nu_+=\nu_s+\nu_i=0$. In this case (Appendix D, case 1), dispersive effects would be canceled here just as they are for the cw-pumped HOM interferometer (Appendix C, case 2), due to the strict anticorrelation imposed on ν_s and ν_i. This anticorrelation is reduced in the pulsed-pump case, and therefore so is the dispersion cancellation.

V. CONCLUSIONS

The calculations presented here show how the dispersive properties of media affect the results of several coincidence photodetection experiments in which the photon pairs are produced by ultrashort pulses. Our analysis focused on those cases for which dispersion cancellation in external media had been found to occur previously with monochromatic (cw) pump sources. We have shown that although the broad spectrum carried by a short pulse generally results in reduced dispersion cancellation, special cases can be found that permit cancellation effects to be maintained even with a broad-band source. In theory, these specially tailored crystal parameters can restore dispersion cancellation and enable certain other quantum interference effects that rely on the suppression of distinguishing mode information for the photons. One implication is that balanced dispersion of any magnitude can be canceled, and need not be a problem for quantum information processing in fibers. Another implication is that for properly chosen crystal parameters, even unbalanced dispersion in the optical elements may be managed without the use of interference filters, while retaining a broad-band pump pulse and its precise classical timing information.

APPENDIX A: THE PHASE-MATCHING FUNCTION FOR COLLINEAR TYPE-I PDC

In type-I PDC the signal and idler beams have similar polarizations [18], and are identically polarized if they propagate collinearly. To perform experiments, the type-I crystal is usually cut and aligned for noncollinear phase matching so that the down-converted beams propagate in slightly different directions and can be manipulated independently. The calculation of phase-matching functions for these noncollinear geometries is complicated [19], and so we will make a simplifying assumption here: because the opening angle between the signal and idler beams is small (typically a few degrees or less), we can neglect the transverse components of their propagation vectors and use a phase-matching function derived for the case of collinear propagation in the direction of the pump beam propagation $\hat{z}$. With the origin for the z axis at the center of the PDC crystal of length L, the phase-matching function is then given by [9]

$$\phi_I(\omega_s,\omega_i)=L\int_{-L/2}^{L/2}dz\,e^{i\Delta kz}, \tag{A1}$$

which yields

$$\phi_I(\omega_s,\omega_i)=L\,\mathrm{sinc}(\Delta kL/2). \tag{A2}$$

The phase mismatch between the pump, signal, and idler waves is

$$\Delta k\equiv k_s(\omega_s)+k_i(\omega_i)-k_p(\omega_s+\omega_i). \tag{A3}$$

This may be expanded about $\overline{\omega}$ to second order to give

$$\Delta k\cong(k_s+k_i-k_p)+\nu_s k_s'+\nu_i k_i'-(\nu_s+\nu_i)k_p'+\tfrac{1}{2}\nu_s^2k_s''+\tfrac{1}{2}\nu_i^2k_i''-\tfrac{1}{2}(\nu_s+\nu_i)^2k_p'', \tag{A4}$$

where $\nu_{s,i}\equiv\omega_{s,i}-\overline{\omega}$ as in Eq. (8). Here k_s, k_i and their derivatives are evaluated at $\overline{\omega}$, while k_p and its derivatives

are evaluated at $2\bar{\omega}$. For collinear type-I PDC, the signal and idler waves are identically polarized, and so

$$k_s' = k_i' = k',$$

$$k_s'' = k_i'' = k''. \tag{A7}$$

With the crystal cut and aligned for collinear phase matching at $\bar{\omega}$, zero-order terms in Eq. (A4) are eliminated. Using the coordinate transformation $\nu_\pm = (1/\sqrt{2})(\nu_s \pm \nu_i)$, we have

$$\tfrac{1}{2}\Delta kL = \tfrac{1}{2} t_+ \nu_+ + \tfrac{1}{4}[(k'' - 2k_p'')\nu_+^2 + k''\nu^2]L, \tag{A8}$$

where

$$t_{+/-} \equiv \frac{1}{2\sqrt{2}}[(k_s' - k_p') \pm (k_i' - k_p')]L. \tag{A9}$$

Because the $k_{s,i,p}'$ correspond to the inverses of the signal, idler, and pump group velocities, the quantity $\sqrt{2}t_+$ is the difference between the time a pump photon takes to traverse the crystal, and the average traversal time for the signal and idler photons. Using Eq. (A7) this can be written in a simpler form

$$t_+ = \frac{1}{\sqrt{2}}(k' - k_p')L. \tag{A10}$$

The difference between the traversal times for the signal and idler photons is $\sqrt{2}t_-$, which is zero for type-I PDC.

Finally, we define the second-order dispersive parameters in the crystal by

$$B = \tfrac{1}{2}k'',$$

$$\bar{B} = \tfrac{1}{2}(k'' - 2k_p''), \tag{A11}$$

so the phase-matching function may be written as

$$\phi_{\mathrm{I}}(\nu_s, \nu_i) = \mathrm{sinc}[(t_+ \nu_+ + BL\nu_+^2 + \bar{B}L\nu_-^2)/2]. \tag{A12}$$

It is easily verified that ϕ_{I} is symmetric under an interchange of signal and idler frequencies, so that

$$\phi_{\mathrm{I}}(\nu_s, \nu_i) = \phi_I^*(\nu_i, \nu_s). \tag{A13}$$

APPENDIX B: THE PHASE-MATCHING FUNCTION FOR COLLINEAR TYPE-II PDC

In type-II PDC, the signal and idler beams have orthogonal polarizations—ordinary or extraordinary—and in practice, both collinear and noncollinear geometries are used. Once again for simplicity we will focus on the collinear phase matching, and refer the interested reader to Ref. [19] for a discussion of the noncollinear case. Just as for the type-I case (Appendix A), we have

$$\phi_{\mathrm{II}}(\omega_o, \omega_e) = L\ \mathrm{sinc}(\Delta kL/2). \tag{B1}$$

In type II PDC our choice of origin results in a simple phase shift proportional to $L(k_o' - k_e')$, which has no physical consequence and is suppressed in the calculation. The notation differs from that in Appendix A in that signal and idler labels (s,i) are replaced by (o,e) for the ordinary and extraordinary polarized modes. Once again we can approximate the phase mismatch term with a Taylor-series expansion about the mean down-conversion frequency $\bar{\omega}$, and write

$$\Delta k \cong k_o + k_e - k_p + k_o'\nu_o + k_e'\nu_e - k_p'(\nu_o + \nu_e), \tag{B2}$$

where $k_{o,e}$ and its derivatives are evaluated at $\bar{\omega}$, k_p and its derivatives are evaluated at $2\bar{\omega}$, and $\nu_{o,e}$ are defined in analogy with $\nu_{s,i}$ in Eq. (8). Unlike the type-I case, only the first-order terms are retained in the expansions of $k(\omega)$ for the type-II phase-matching function. This is because the first-order terms (corresponding to the group velocities of the orthogonally polarized signal and idler in the PDC) no longer cancel, and are much larger than the higher-order terms.

Proceeding as in Appendix A, we eliminate the zero-order terms in Eq. (B2) and use a coordinate transformation $\nu_\pm = (1/\sqrt{2})(\nu_o \pm \nu_e)$ to write

$$\phi_{\mathrm{II}}(\nu_o, \nu_e) = \mathrm{sinc}[(t_+ \nu_+ + t_- \nu_-)/2], \tag{B3}$$

where $t_\pm$ are defined in analogy with Eq. (A9). Note that this PMF is not symmetric under interchange of the o and e frequencies:

$$\phi_{\mathrm{II}}^*(\nu_e, \nu_0) = \mathrm{sinc}[(t_+ \nu_+ - t_- \nu_-)/2]. \tag{B4}$$

APPENDIX C: LIMITING CASES OF INTEREST FOR TYPE-I HOM INTERFERENCE

Case 1: Recovery of interference in the limit of no external dispersion

We note that in the absence of external dispersion, ($\beta = 0$), Eq. (19) yields the HOM interference coincidence-count profile for pulsed type-I PDC without any spectral filters,

$$R_n^I(\bar{\tau}) = 1 - \frac{1}{C}\int_0^1 dz\, \frac{1-z}{\sqrt{z}} \cos\left[\frac{2\bar{\tau}^2}{k''Lz} - \frac{\pi}{4}\right] e^{-[(1/2)\sigma t_+ z]^2}, \tag{C1}$$

where we have made use of Eq. (A11). This result is identical to that of Ref. [10], but the spectral width (σ) bears an inverse relation to the temporal width used in that reference.

Case 2: Recovery of interference in the cw-pumped limit

We expect to recover dispersion cancellation effects in the cw-pumped limiting case where the pump bandwidth σ goes to zero. The pump spectral profile then becomes

$$\alpha(\nu_s + \nu_i) \propto \delta(\omega_s + \omega_i - 2\varpi). \tag{C2}$$

This limit corresponds to a purely monochromatic pump of frequency $2\bar{\omega}$. The integration of the δ function over either frequency variable in Eq. (12) enforces perfect anticorrela-

tion and frequency entanglement ($\nu_s = -\nu_i$) about the degenerate center frequency. This result eliminates the GVD terms containing β in Eq. (12) so dispersion cancellation effects are recovered. This anticorrelation would not cancel any odd-ordered terms had they been retained in the expansion of $\kappa(\nu_{s,i})$.

We note also that the plot of our coincidence rate for low σ in Fig. 5 matches the form of the coincidence data observed in the cw-pumped experiment of Ref. [8], where no spectral filters were used.

Case 3: Spectral filters and their narrow-band limit

Spectral band-pass filters can be included in the type-I HOM calculation in the same way they were included in Eq. (29) for the noninterferometric case. Gaussian spectral filters centered at $\overline{\omega}$, with bandwidth σ_F are modeled by inserting the following product term into the integrand of Eq. (13):

$$\exp(\nu_s^2/\sigma_F^2)\exp(\nu_i^2/\sigma_F^2) = \exp[(\nu_+^2 + \nu_-^2)/\sigma_F^2]. \quad \text{(C3)}$$

This leads to a final integral with a form identical to that of Eq. (19), provided that Ω_z is replaced with Ω_{zF},

$$\frac{1}{\Omega_{zF}^2} = \frac{1}{\Omega_z^2} + \frac{1}{\sigma_F^2} \quad \text{(C4)}$$

and that B is replaced with B_F,

$$B_F = B + \frac{i}{\sigma_F^2 L z}. \quad \text{(C5)}$$

These substitutions permit Eq. (19) to include the effects of band-pass filters. Inspection of that equation then shows that in the limit of narrow bandwidth, filter effects predominate over pump and crystal parameters. On the other hand, a large filter bandwidth has a negligible effect on the calculation (as we would expect).

If we insert extremely narrow spectral filters before the detectors, the phase-matching function can be suppressed and Eq. (13) may be approximated by

$$R^I(\overline{\tau},\beta) \propto \int_{-\infty}^{\infty}\int_{-\infty}^{\infty} d\nu_s d\nu_i e^{-(\nu_s+\nu_i/\sigma)^2} \times e^{-(\nu_s/\sigma_F)^2} e^{-(\nu_i/\sigma_F)^2} \times \{1 - e^{i[(\nu_s-\nu_i)\overline{\tau} + \beta l(\nu_s^2 - \nu_i^2)]}\}. \quad \text{(C6)}$$

Because

$$\lim_{\sigma_F \to 0} [e^{-(\nu_{s,i}/\sigma_F)^2}] \propto \delta(\nu_{s,i}), \quad \text{(C7)}$$

the effect of very narrow filters is to introduce the product of two δ functions, $\delta(\nu_s)\delta(\nu_i)$, thereby constraining *both* ν_s and ν_i to very small values by postselecting only degenerate center frequency photons for detection. This differs significantly from the limiting case of Eq. (21) in which a source PMF of the form $\delta(\nu_s - \nu_i)$ constrains only the frequency *difference* for the pair.

Case 4: Recovery of cancellation with balanced dispersion

''Balanced dispersion'' occurs when identical dispersive elements are placed in both arms of the HOM interferometer in Fig. 3. Previous analyses for both the cw [7] and pulsed [14] pump cases predicted the cancellation of dispersive effects to *all* orders, not just the even orders as with a single element. This effect can easily be seen by inserting the additional phase term for the second medium into the signal field operators expansion of Eq. (5): the coincidence rate in Eq. (6) would then become

$$R(\tau) \propto \int_0^{\infty}\int_0^{\infty} d\omega_s d\omega_i |\alpha(\omega_s+\omega_i)|^2 \{|\phi(\omega_s,\omega_i)|^2 - \phi(\omega_s,\omega_i)\phi^*(\omega_i,\omega_s) \times e^{i[(\omega_s-\omega_i)\tau + [\kappa(\omega_s)-\kappa(\omega_i)]l + [\kappa(\omega_i)-\kappa(\omega_s)]l]}\} \quad \text{(C8)}$$

so that the dispersive phases accumulated in each arm cancel each other identically. This quantum-mechanical effect contrasts with the dispersive broadening that would be predicted classically. There are practical implications for experiments utilizing short pulses in which the interferometric paths copropagate or are constructed with matched pairs of long single-mode optical fibers. Besides taking advantage of flexible long-range signal relay and high modal overlap, an interferometer could be operated at frequencies where photon counting is optimal but fiber dispersion is high, without loss of interference visibility or temporal resolution.

APPENDIX D: LIMITING CASES OF INTEREST FOR THE NONINTERFEROMETRIC ARRANGEMENT

Case 1: $\sigma = 0$ (cw pump)

The dispersive effects are cancelled and Eq. (30) reduces to

$$R(\tau) \propto \exp(-\tau^2\sigma_F^2) \quad \text{(D1)}$$

as in Ref. [6]. The width of this Gaussian profile ($1/\sigma_F$) is determined solely by the filter bandwidth, as if no dispersion were present.

Case 2: $0 < \sigma_F \ll \sigma$, and $\sigma_F \ll \beta l$ (ultranarrow band filter)

This limit of Eq. (30) again yields Eq. (D1), provided that linear offsets in τ due to the mean propagation time within the dispersive media are neglected. Once again, the width of the temporal profile of the coincidence counting rate is $1/\sigma_F$, with second-order dispersive effects (β) canceled. This limit is also in agreement with Ref. [6].

Case 3: $0 < \sigma \ll \sigma_F$ (filter width much greater than a nonvanishing pump spectrum)

The coincidence rate reduces to

$$R(\tau) \propto \exp[-\tau^2/(\sigma\beta l)^2]. \quad \text{(D2)}$$

Though the pump spectrum is small, the signal and idler photons still have large bandwidth. The width of the temporal profile is now given by $\sigma\beta l$. Hence either a larger pump spectrum σ (shorter pulse) or a greater dispersive phase βl yields temporal broadening of the coincidence count profile. Thus there is no dispersive cancellation in this case.

ACKNOWLEDGMENTS

We thank Brian E. King for his thorough reading of this manuscript. This work was supported by the National Science Foundation, by the Air Force Research Laboratory and the Army Research Office (R.E.), and by the Office of Naval Research and the Rochester Theory Center (D.B.).

[1] R. L. Freeman, *Telecommunications and Transmission Handbook*, 2nd ed. (Wiley Interscience, New York, 1998).
[2] W. Tittle, J. Brendel, H. Zbinden, and N. Gisin, Phys. Rev. Lett. **81**, 3563 (1998).
[3] J. W. Pan, D. Bouwmeester, H. Weinfurter, and A. Zeilinger, Phys. Rev. Lett. **80**, 3891 (1998).
[4] S. L. Braunstein and A. Mann, Phys. Rev. A **51**, R1727 (1995).
[5] C. K. Hong, Z. Y. Ou, and L. Mandel, Phys. Rev. Lett. **59**, 2044 (1987).
[6] J. D. Franson, Phys. Rev. A **45**, 3126 (1992).
[7] A. M. Steinberg, P. G. Kwiat, and Y. Chiao, Phys. Rev. A **45**, 6659 (1992).
[8] A. M. Steinberg, P. G. Kwiat, and Y. Chiao, Phys. Rev. Lett. **68**, 2421 (1992).
[9] W. P. Grice and I. A. Walmsley, Phys. Rev. A **56**, 1627 (1997).
[10] T. E. Keller and M. H. Rubin, Phys. Rev. A **56**, 1534 (1997).
[11] Z. Y. Ou, Quantum Semiclass. Opt. **9**, 599 (1997).
[12] D. Bouwmeester, J. W. Pan, K. Mattle, M. Eibl, H. Weinfurter, and A. Zeilinger, Nature (London) **390**, 575 (1997).
[13] M. Zukowski, A. Zeilinger, and H. Weinfurter, Ann. N.Y. Acad. Sci. **755**, 91 (1995); A. Zeilinger, M. A. Horne, H. Weinfurter, and M. Zukowski, Phys. Rev. Lett. **78**, 3031 (1997).
[14] J. Perina, Jr., A. V. Sergienko, B. M. Jost, B. E. A. Saleh, and M. C. Teich, Phys. Rev. A **59**, 2359 (1999).
[15] L. Mandel and E. Wolf, *Optical Coherence and Quantum Optics* (Cambridge University Press, Cambridge, England, 1995).
[16] D. N. Nikogosyan, Appl. Phys. A: Solids Surf. **52**, 359 (1991).
[17] B. E. A. Saleh and M. C. Teich, *Fundamentals of Photonics* (Wiley, New York, 1991).
[18] A. Migdall, J. Opt. Soc. Am. B **14**, 1093 (1997).
[19] N. Boeuf, D. Branning, I. Chaperot, E. Dauler, S. Guerin, G. Jaeger, A. Muller, and A. Migdall, Opt. Eng. (Bellingham) **39**, 1016 (2000).